

Chapter 3

Frictional Strength and the Effective Pressure Law of Montmorillonite and Illite Clays

C. Morrow, B. Radney¹, and J. Byerlee
U. S. Geological Survey, Menlo Park, CA 94025, U. S. A
¹*Now at Amoco Oil Co., Houston, Texas, U.S.A.*

Abstract

Low-strength clay minerals are a common constituent of fault gouges, and are often cited as a possible explanation for the low ambient shear stresses along the San Andreas fault inferred from heat flow constraints and in situ stress measurements. Montmorillonite, the weakest of the clay minerals, undergoes a gradual phase transition to illite with depth. In order to compare the shear stresses supported by these two minerals with those thought to exist along the San Andreas, we have measured the frictional sliding behavior of pure montmorillonite, mixed montmorillonite/illite and pure illite as a function of effective pressure, simulating burial to seismogenic depths. Strength measurements verify that the effective pressure law for friction holds for these minerals under all conditions. That is, the measured stresses were a function of the effective pressure, $P_c - P_p$, independent of the choice of confining and pore pressure. This relation, common for many other rock types, was previously untested for these clays under most conditions. Results show that dry samples were consistently stronger than saturated samples, and that strength increased with increasing illite content. In addition, the coefficient of friction increased as a function of pressure for the montmorillonite gouge, but was independent of pressure for the illite gouge. This behavior may be explained by the presence of loosely bonded interlayer water in the montmorillonite, which is squeezed out at higher pressures, changing the frictional characteristics of the clay. The nonexpanding illite was not affected in this way. For the montmorillonite-to-illite compositional profile, an average shear stress of 60 MPa was determined for crustal conditions to 15 km, assuming a normal hydrostatic gradient. If montmorillonite remains stable at depth, the resulting average shear stress is reduced to 30 MPa. In either case, these values are above the 10-20 MPa shear stress limit along the San Andreas inferred from heat flow constraints. Strength may be reduced to in-situ levels if fluid pressures become greater than hydrostatic within the gouge zone.

1. Introduction

It has long been recognized that the mechanical properties of clay-rich materials are pertinent to the discussion of fault zone behavior. Many varieties of clay minerals are commonly found in fault gouges along the San Andreas and other major active faults. These minerals are thought to persist to seismogenic depths, on the basis of geochemical and geophysical evidence such as velocity and density profiles (Wu et al., 1975; Wang, 1984). Clay minerals are consistently weaker than natural rock-flour gouges composed of crushed granitic material (Morrow et al., 1984). Anomalously low frictional strength is often cited as a possible factor in the long-standing stress-heat flow debate. This debate has arisen because the strength of typical crustal rocks measured in the laboratory is inconsistent with the low strength of the San Andreas fault inferred from in-situ measurements and the lack of a frictionally generated heat flow anomaly (Lachenbruch and Sass, 1980). Conductive heat flow measurements in numerous shallow boreholes near the fault imply an average shear stress level of 10-20 MPa, at least an order of magnitude below that implied by the laboratory strength data for nonclay rock gouges. Although the stress-heat flow debate, in which gouge strength is only one aspect, has not been fully resolved, it has led to numerous studies of the frictional properties of clays.

The expandable clay, montmorillonite, is by far the weakest of the clay minerals commonly found in fault zones and as such, is of particular interest to the discussion of fault strength. This clay typically undergoes a gradual dehydration and phase change to the stronger, nonexpandable clay, illite, with increasing temperature and pressure. The two minerals coexist as a mixed-layer phase at intermediate states of the diagenesis process. This phase transition is well documented in hydrothermally altered rocks, contact metamorphic environments, and sedimentary basins such as the Gulf Coast of North America. The temperatures and pressures at which diagenesis begins and ends depend on a number of factors including composition of the original clay, chemistry of available fluids, porosity and geologic environment (Freed and Pecor, 1989; Colten-Bradley, 1987; Meunier and Velde, 1989). Generally, the transition begins at temperatures less than 100°C, as in the case of the Gulf Coast. However, Wu et al. (1975), Wang (1984), and others suggest that in certain environments montmorillonite may be stable to 300-400°C, corresponding to seismogenic depths in the earth. If this weak mineral persists at depth, then its deformation behavior may be important to the understanding of fault dynamics.

Numerous frictional sliding studies of montmorillonite yield a wide range of reported strengths, largely because of the strong influence of fluids on this highly expandable clay. Reported shear stresses vary depending on whether the clay is in the dry or saturated state, the degree of saturation, and whether overpressured fluids have been unintentionally generated due to the low permeability of the clay (Summers and Byerlee, 1977; Byerlee, 1978; Wang et al., 1979; Wang and Mao, 1979; Morrow et al., 1982). As a result, the manner in which the strength of montmorillonite varies with effective pressure is not well known. For this reason, we have undertaken a series of frictional sliding experiments in which care has been taken to maintain pore pressure without generating overpressured fluids. In particular, we wish to study the important case in which pore pressure varies with depth according to the hydrostatic gradient. The choice of samples represents two different scenarios for the composition of a fault zone. The first assumes that montmorillonite persists to seismogenic depths. The strength of pure montmorillonite was measured under a series of confining and pore pressures simulating

depths of burial from 0 to 15 km. The second case assumes that montmorillonite undergoes a phase change to illite with increasing pressure. For these tests, a mixture of montmorillonite and illite was used at intermediate pressures, representing a mixed layer phase, and pure illite was tested at the higher pressures, simulating the completion of diagenesis. In this way the average shear stress values of the two compositional profiles can be compared with the 10-20 MPa shear stress level thought to exist along the San Andreas fault. The magnitude of these shear stresses will indicate whether or not low-strength clay minerals are sufficient to explain the existence of a weak fault.

2. Effective Pressure Law for Friction

In order to report the true strength of these gouges as a function of effective pressure, we need to determine the proper form of the effective pressure relation for friction. With the exception of experiments conducted on montmorillonite at 100 MPa by Wang and Mao (1979), this point has not been specifically tested for the clay minerals used in this study. Accordingly, an investigation of the effective pressure law forms the second major focus of this chapter.

The effective pressure is usually defined as

$$P_e = P_c - \alpha P_p \quad (1)$$

where P_e is the effective pressure, P_c is the confining pressure, α is a parameter that incorporates the physical properties of the rocks, and P_p is the pore pressure. This equation can also be written in terms of the effective stress, σ_e , where the effective stress is equivalently defined as

$$\sigma_e = \sigma - \alpha P_p \quad (2)$$

This form is relevant to the discussion of friction, where the applied normal stress on a slip surface is reduced by the fluid pressure. The parameter α in these equations has been analytically derived for certain elastic rock properties. See, for example, Nur and Byerlee (1971), Robin (1973) and Garg and Nur (1973), among others. It should be noted that the effective pressure need not vary linearly with confining and pore pressure, and that it may not have a simple analytic expression.

Generally, α is determined empirically for a particular rock property and rock type, yielding values between 0 and 1. The larger the value of α , the more dependent the effective pressure is on the fluid pressure. When $\alpha = 1$, eq. (1) reduces to the more common form

$$P_e = P_c - P_p \quad (3)$$

This expression has been found to be approximately correct for many properties of brittle rocks (Brace, 1972).

The effective pressure law for friction has been studied for a number of materials. Byerlee (1967) found that the effective pressure law (3) held for the sliding of granite at room temperature. Deviations from this law in crystalline rocks have been linked to dilatancy and strain rate-dependent pore pressure, where the true pore pressure in the rock may be different from the externally measured pore pressure (Brace and Martin, 1968; Garg and Nur, 1973). Moore et al. (1984a,b) studied the friction of granite, serpentinite, and clay gouges at a variety of temperatures. They found a deviation from

the effective pressure law for the serpentine and sheet silicate gouges, possibly because pore fluids became trapped and overpressured during shearing. It is important to determine whether these gouges follow the effective pressure law under drained conditions, where over- or underpressured fluids are not generated, as was observed in the experiments noted above. In addition, expandable clays such as montmorillonite contain loosely bonded interlayer water whose role in relation to the effective pressure law is unknown. Does this bonded water interact with the free water in a way that may alter the effective pressure law? Does the strength depend on how many bonded layers are present, or on the bonding strength of each layer?

These questions must be answered before the true state of stress in the experiments can be determined. For this reason, the strengths of the three gouge types were studied under many combinations of confining and pore pressures, in addition to those representing a normal lithostatic-to-hydrostatic ratio, so that the effective pressure law could be fully investigated. We wish to address several main points: What are the shear strengths of these clays as a function of effective pressure? What is the form of the effective pressure law for friction that is required to describe these materials? Finally, is there some difference between the expandable and nonexpandable clays that may influence the frictional characteristics of the samples?

3. Sample Description and Procedure

The samples used in this study consisted of fine-grained particles of montmorillonite, illite, and a 50% by weight mixture of these two clays. The montmorillonite was a commercially obtained powder (Volclay SPV-200), with 65% of the grains finer than 200 mesh (74 μm). The illite gouge was obtained by crushing a natural shale from Fithian, Illinois.

The clay gouges were saturated with distilled water to form a thick paste using the same weight of clay and water in each case. A 1 mm-thick layer of the saturated gouge was placed between the surfaces of a 2.5 cm diameter cylindrical sample, cut at an angle of 30° as shown in Figure 1. The upper half of this sample was composed of Berea Sandstone, the lower half of fused silica, with a total length of 6.3 cm. The Berea Sandstone has a porosity of 18%, and a permeability of around 10^{-13} m^2 along the direction of bedding (Zoback and Byerlee, 1975). This permeability is about eight orders of magnitude higher than the permeability of the clay layer ($\sim 10^{-21} \text{ m}^2$; Morrow *et al.*, 1984) at the pressures of these experiments. Fused silica was used in the bottom section because of the low permeability of the clay gouges, which would cause a long time delay in the saturation of the bottom section if it were composed of sandstone. In addition, pore volume reduction during deformation could create excess fluid pressures which become trapped beneath the low-permeability clay layer. The impermeable fused silica eliminates these problems by preventing fluids from entering the bottom section entirely, where the pore pressure cannot easily be monitored. The highly permeable Berea Sandstone on the upper half insured close communication between fluids in the rock and those in the fluid pressure generator and pore pressure transducers. Each rock-glass assembly was held together with a copper foil jacket (0.05 mm thick), and placed in a vacuum oven at 100°C for 24 hours to dry the samples. The copper foil tears easily during shearing, and does not affect the strength measurements. After drying, the samples were then placed in a polyurethane jacket and fastened to the steel endplugs

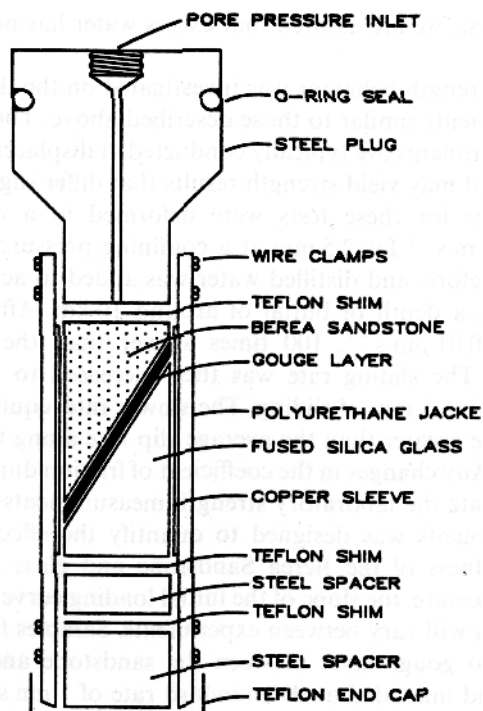


Figure 1. Sample assembly.

with wire clamps. Since the two halves of each sample must move slightly sideways during shearing, lubricated shims were added at the interfaces of the sample column to minimize frictional resistance in the horizontal direction.

All frictional sliding experiments followed the same deformation history, under a wide range of confining and pore pressures, to produce effective pressures of 1, 2, 20, 30, 50, 100, 150, 200, 300, and 400 MPa. All pressures and displacement rates were maintained by computer-controlled servomechanisms. Pressure measurements were accurate to 0.05 MPa, displacement to 10^{-6} m. At the start of each run, the pore fluid lines were evacuated to remove all water in the system. Confining pressure was applied and sliding initiated at an axial displacement rate of $0.866 \mu\text{m s}^{-1}$. This corresponds to a shear displacement rate along the inclined gouge layer of $1 \mu\text{m s}^{-1}$. After 2.5 mm of axial displacement, the piston was held fixed for 10 000 s. Distilled water was then introduced to the sample and pore pressure was raised to the desired level where it was left to equilibrate for the duration of the pause. Thereafter, sliding continued at the previous rate of $1 \mu\text{m s}^{-1}$ to a maximum value of 7 mm. In some experiments the sample was left dry throughout. The purpose of the dry/wet procedure was to assure that the fluid in the gouge layer did not become overpressured owing to the initial loading of the sample. Most of the pore volume reduction occurs during this phase. If the permeability of the gouge layer is particularly low, then fluids may not be expelled fast enough to maintain the desired pore pressure. In that case, we could not determine true effective pressure acting on the sample. By introducing the fluid after the sample is

already under shear stress, we are assured that excess water has not become trapped in the gouge.

Velocity-dependent strength behavior was investigated on the three gouge types with frictional sliding experiments similar to those described above. These tests are pertinent because laboratory experiments are typically conducted at displacement rates faster than those of active faults, and may yield strength results that differ slightly from true in-situ conditions. The samples for these tests were deformed in a dry state at a shear displacement rate of $1 \mu\text{m s}^{-1}$ for 2.5 mm at a confining pressure of 300 MPa. Sliding paused for 10 000 s as before, and distilled water was added to achieve a pore pressure of 100 MPa, simulating a depth of burial of around 10 km. After saturation, sliding resumed at a rate of $0.01 \mu\text{m s}^{-1}$, 100 times slower than the previous rate, to a displacement of 7 mm. The sliding rate was then increased to the original value of $1 \mu\text{m s}^{-1}$ for the remaining 1 mm of sliding. The slower rate, equivalent to 31 cm/year, is an order of magnitude greater than the average slip rate along the San Andreas fault of around 2.5 cm/year. Any changes in the coefficient of friction during these experiments can be used to extrapolate the laboratory strength measurements to in-situ conditions.

A final set of experiments was designed to quantify the effects of elastic stiffness. Because the elastic stiffness of the Berea Sandstone and glass sample configuration depends on confining pressure, the slope of the initial loading curve and the displacement at which sliding initiates will vary between experiments. Samples for these stiffness tests were assembled with no gouge layer between the sandstone and glass surfaces. The samples were loaded and unloaded at the standard rate of $1 \mu\text{m s}^{-1}$ several times to a maximum displacement of 1 mm. This computer-controlled procedure was repeated at all the confining pressures used in the frictional sliding experiments. The results of these tests were used to derive the true shear displacement for each sample, so that experiments at different pressures could be compared. As a part of the stiffness testing procedure, the seal friction of the machine was also determined by cycling the piston back and forth under pressure while not in contact with the sample. This friction is the force needed to slide the piston past the O-ring seal assembly. Since axial force is measured outside the pressure vessel, the true axial force on the sample must be corrected for this friction.

4. Results

4.1. Dry runs

Shear stress versus axial displacement for selected dry runs is shown in Figure 2. The stress data are corrected for the decreasing area of contact as the two sawcut surfaces slide past one another. This decreasing area results in an increase in the normal stress during shearing. Confining pressures of 30, 150, and 300 MPa represent depths of burial of 1, 5, and 10 km, respectively. This plot shows data for all three gouge types, with data for the illite and mixed clay at the higher pressures only, representing the greater depths at which they would be expected to occur in nature. Shear stresses rose rapidly during the initial elastic portion of the curves, then continued to rise more slowly as the samples began to slide. At 2.5 mm displacement, the stresses dropped slightly during the 10 000 s pause, owing to creep in the sample under the sustained load. This behavior is typical of granular materials under stress (Morrow and Byerlee, 1989). When sliding

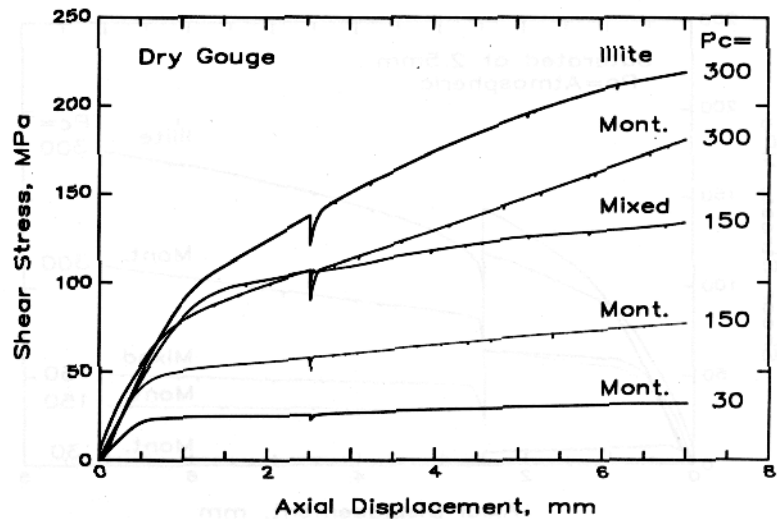


Figure 2. Shear stress as a function of axial displacement for vacuum-dried samples of pure montmorillonite, mixed montmorillonite/illite, and pure illite gouges. Confining pressures are indicated at right in MPa. The drop in shear stress at 2.5 mm corresponds to the 10 000 s pause in sliding.

was resumed, the shear stresses quickly rose to the previous level as if there had been no interruption. The relative strength of the gouges at a particular pressure was dependent on the amount of montmorillonite present, which is the weaker of the constituent minerals. In addition, the samples all strain hardened with displacement. The gradual increase in strength is a function of confining pressure, with more strain hardening observed at the higher pressures than at the lower. This observation is consistent with the strain hardening behavior of numerous other clay-rich fault gouges collected along the San Andreas and nearby faults (Morrow et al., 1982). Clearly, the reported strength of these gouges depends on how far the samples have slid if strain hardening behavior is observed. With the exception of the illite, whose strain hardening rate began to decrease near the end of the experiment, we have not slid far enough to observe any changes in the displacement-dependent behavior that may indicate how the samples will behave at large shear strains. Owing to the geometric limitations of the triaxial system, such large-strain behavior would be better observed in a rotary shear apparatus.

4.2. Saturated runs

Several dozen runs were conducted with saturated gouge at a variety of confining and pore pressures on the illite, montmorillonite, and mixed clays. Figure 3 shows the effects of saturation for the same gouges and confining pressures discussed in Figure 2. For these runs, distilled water was injected into the sample during the 10 000 s pause, and held at atmospheric pressure after the onset of shearing, so that the effective pressure was unchanged before and after the pause. Shear stresses increased during the dry portion as before. However, the strength increases were not entirely reproducible, particularly for the expandable montmorillonite, because of slight variations in the atmospheric humidity absorbed by the clay before the experiment. The introduction of

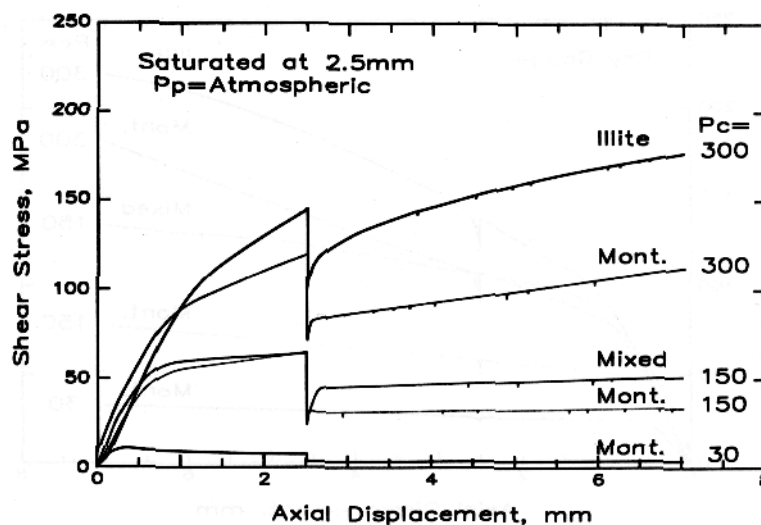


Figure 3. Shear stress as a function of axial displacement for the same gouges and stress conditions as shown in Figure 2. During the 10 000 s pause at 2.5 mm, distilled water was introduced at atmospheric pressure. Confining pressures are shown at right in MPa.

water during the pause equalized these differences, and also caused a reduction in the shear stress even more pronounced than the decrease observed during the pause in the dry runs. When sliding resumed, the samples did not regain the former shear stress levels, as was observed for the dry samples. In addition, the strain hardening rate was significantly reduced for samples at the highest pressure (300 MPa), from around 30 to 8 MPa mm^{-1} for the illite and from 16 to 7 MPa mm^{-1} for the montmorillonite. At lower pressures, the gouges slid at a steady-state shear stress level with little or no strain hardening. These tests verify that the presence of fluids decreased the strength and strain hardening of the gouges even though the applied pressure remained unchanged.

Petrographic observations of both the wet and dry samples show textural evidence for the strength differences. The deformation fabric of the dry samples for all three of the gouge types was much more developed than that of the wet samples at the same pressure. At 30 MPa, the dry sample contained boundary shear zones along both sawcut interfaces, in which clay platelets were aligned parallel to the direction of shearing. At 150 MPa this shear zone encompassed the entire width of the sample, and at 300 MPa kink bands within the fabric were prominent. In contrast, deformation in the saturated samples at the lower pressures was confined to a few boundary layers and Riedel shear bands, separated by large areas of undeformed gouge. Only at 300 MPa did the samples show evidence of deformation throughout the entire gouge layer.

The strength of the saturated gouge was further affected when pore pressure was increased from atmospheric to near lithostatic values. Figure 4 shows the shear stress as a function of axial displacement for montmorillonite at a constant confining pressure of 150 MPa. After the pause, fluids were added at pressures of 0.1, 50, 100, and 148 MPa, with a resulting decrease in strength for each increase in pore pressure. This behavior is to be expected, as the effective confining pressure acting on the sample is gradually reduced. This figure illustrates how readily the strength of the gouge can decrease to very low values in the natural environment if the fluid pressure is increased. The mixed

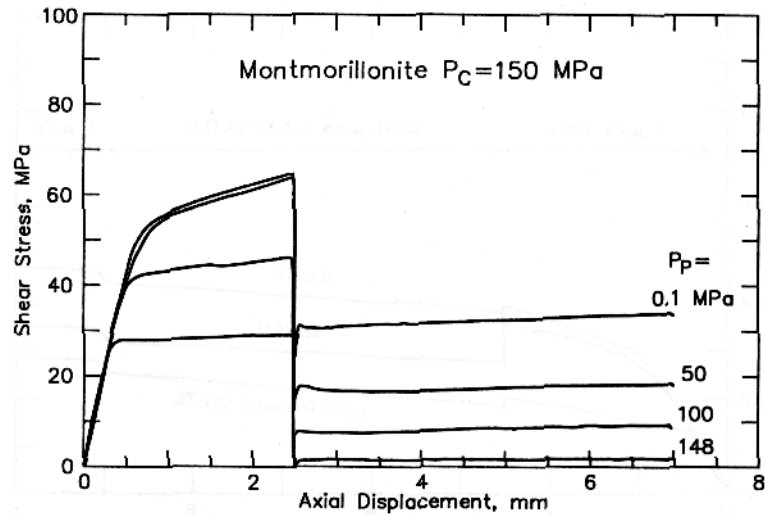


Figure 4. Shear stress as a function of axial displacement for the pure montmorillonite gouge at a confining pressure of 150 MPa. Increasing pore pressure reduces the strength.

clay and pure illite samples behaved in a similar fashion, although the drop in strength was less pronounced as montmorillonite content decreased. Note that the dry and wet portions of the strength curves are no longer directly comparable since they are not at the same stress state. Further discussions of strength will concentrate on the stress measurements taken after the pause at 2.5 mm. Figure 4 is an example of the numerous stress plots produced as a function of confining and pore pressure which were needed to investigate the strength of the clays as a function of effective pressure. These other plots have been omitted for brevity, as the stress values at different pressure conditions can be derived from the effective pressure analysis discussed below.

4.3. Velocity dependence

In order to determine whether these laboratory strength measurements are comparable to the in-situ conditions, a velocity step test was conducted for each of the gouges at confining and pore pressures of 300 and 100 MPa, respectively, representing a depth of burial of around 10 km. The resulting coefficients of friction are plotted as a function of displacement in Figure 5. The true change in strength of the gouge is masked at the first velocity step (2.5 mm) because of the decrease in strength due to saturation. Therefore, the relevant portion of this plot is at 7 mm, where the sliding velocity changes by a factor of 100 from $0.01 \mu\text{m s}^{-1}$ to $1 \mu\text{m s}^{-1}$ as measured along the inclined gouge layer. The coefficient of friction increased for all of the samples by about 0.025, indicating a velocity-strengthening behavior. This increase was 5-8% of the total coefficient of friction at 7 mm displacement.

The velocity dependence of friction can be defined following Logan and Rauenzahn (1987) as

$$a - b = \frac{d\mu}{d(\ln(\dot{\delta}))} \quad (4)$$

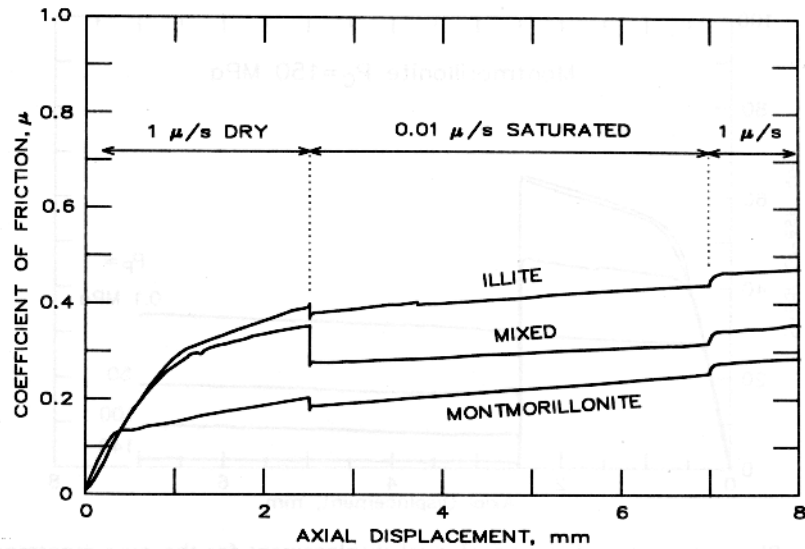


Figure 5. Coefficient of friction as a function of axial displacement at 300 MPa confining pressure and 100 MPa pore pressure. The sample was saturated at 2.5 mm; slip rates along the gouge layer are indicated above the curves.

where a is the initial response to the velocity change, b is the magnitude of the decay to the steady-state value, μ is the steady-state coefficient of friction, and δ is the displacement rate. The $a - b$ values for these experiments were 0.005 for both the montmorillonite and illite samples, and 0.007 for the mixed clay. These values are consistent with the findings of Logan and Rauenzahn (1987) on experiments with pure montmorillonite. Therefore, the velocity dependence of friction does not appear to be affected by the expandable or non-expandable nature of the clays. If we assume an average slip rate on the San Andreas fault of 2.5 cm/year, or $7.9 \times 10^{-7} \text{ mm s}^{-1}$, then the slower rate of the step test was around one order of magnitude higher than the San Andreas rate. We would therefore expect a further few percent reduction in shear strength for samples deformed at these rates. Such low-velocity experiments are not practical in the laboratory because of time constraints, and were not used to investigate the effective pressure law, but they are relevant to the discussion of the strength of natural faults.

4.4. True shear displacement

In order to test the effective pressure law for friction, the shear and normal stress values of the different samples must be compared at the same shear displacement. This is necessary because the elastic stiffness of the sample column is a function of confining pressure, and therefore the point at which sliding commences varies between experiments. From the load and displacement data of the gouge-free sample, elastic stiffnesses were calculated ranging from 271 to 317 MPa mm⁻¹. Stiffness increased with confining pressure at 300 MPa. At 400 MPa, grain crushing within the Berea Sandstone reduced the stiffness of the sample. These data were used to calculate the shear displacement

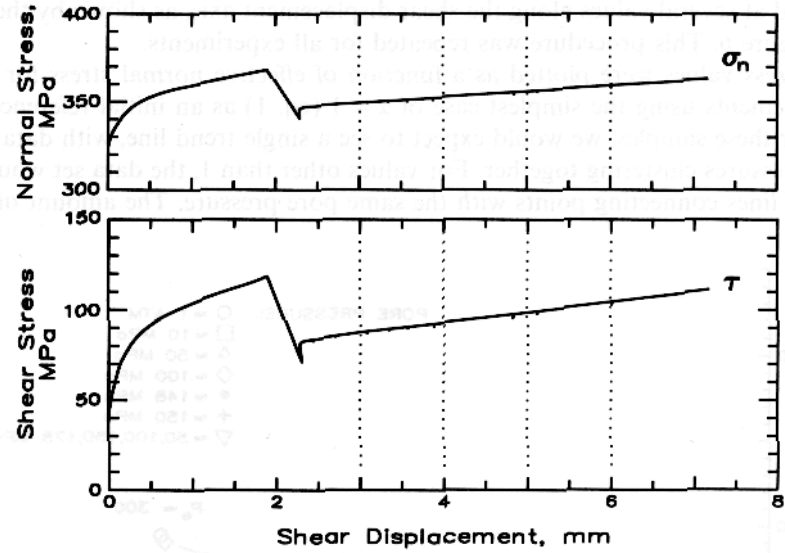


Figure 6. Shear and normal stress as a function of shear displacement for the montmorillonite gouge at a confining pressure of 300 MPa and atmospheric pore pressure. The data have been modified to normalize the elastic stiffness of the machine and rock cylinder under different pressures, and resolve the axial displacement along the inclined gouge layer.

along the gouge layer at each confining pressure, defined as

$$dl = \frac{dz}{\cos \theta} - \frac{\Delta\sigma}{K \cos \theta} \quad (5)$$

where

dz = axial displacement (mm)

$\Delta\sigma$ = differential stress (MPa), corrected for the decreasing area of contact during sliding

K = elastic stiffness of the gouge-free sample (MPa mm^{-1})

This calculation resolves the displacement along the gouge layer (first term) and shifts the data along the displacement axis to normalize the elastic portion of the deformation (second term). With this normalization, the shear stress values can be compared at the same displacement for experiments run at equivalent effective pressures but widely varying confining and pore pressures. This displacement correction does not account for compaction of the gouge during shearing; however, most of the compaction takes place during the initial loading of the sample.

Figure 6 illustrates the data normalization for the montmorillonite gouge at a confining pressure of 300 MPa and atmospheric pore pressure shown in Figure 3. Shear and normal stresses are plotted as a function of the shear displacement parallel to the fault. This plot shows the true deformation in the gouge layer, rather than the deformation observed external to the loading apparatus. As a consequence, the initial elastic loading curve is steeper, and the sloping trend during the 10 000 s pause reflects the creep and stress relaxation in the sample under the sustained load. Shear and normal stress values

were picked at several values along the shear displacement axis, as shown by the dotted lines in Figure 6. This procedure was repeated for all experiments.

Shear stress values were plotted as a function of effective normal stress for each of the displacements using the simplest case of $\alpha = 1$ (eq. 1) as an initial reference point. If $\alpha = 1$ for these samples, we would expect to see a single trend line, with data for like effective pressures clustering together. For values other than 1, the data set would form a family of lines connecting points with the same pore pressure. The amount of spread

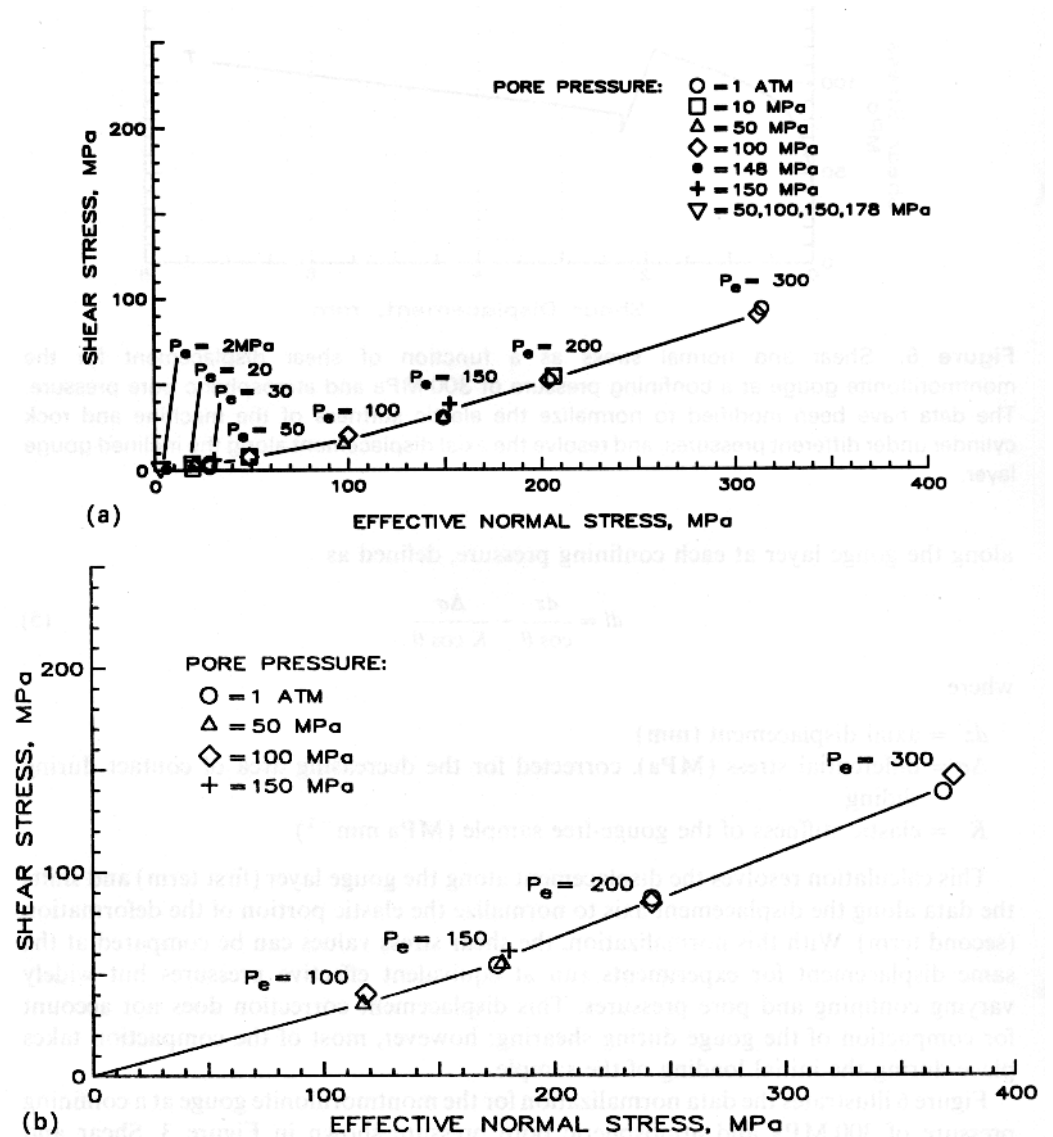


Figure 7. (a) Shear stress as a function of effective normal stress for the montmorillonite gouge at a shear displacement of 4 mm. Effective normal stress $P_c - \alpha P_p$, calculated with the coefficient $\alpha = 1$. Pore pressures are indicated by symbols at right. (b) Shear versus effective normal stress ($P_c - \alpha P_p$), for the mixed montmorillonite/illite gouge at shear displacement of 4 mm with the coefficient $\alpha = 1$.

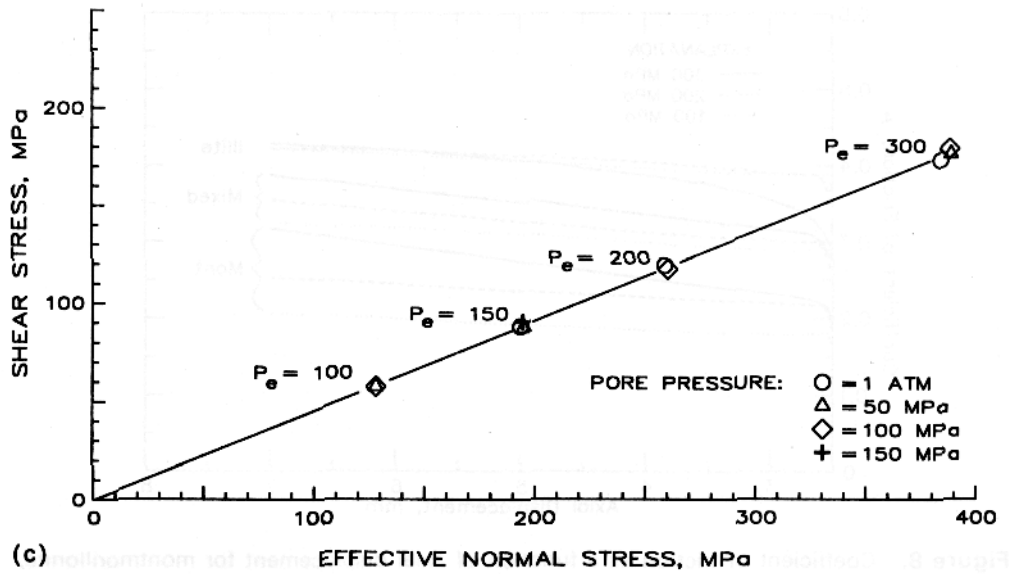


Figure 7. Continued. (c) Shear versus effective normal stress ($P_c - \alpha P_p$) for the illite gouge at shear displacement of 4 mm with the coefficient $\alpha = 1$.

in the lines would indicate the magnitude of the correction in a required to bring the data into a single line. Figures 7a-c show examples of these plots for the three gouge types at 4 mm shear displacement. Pore pressures are indicated by the symbols, and confining pressures for each experiment can be determined by adding the pore pressure to the stated effective pressure. Data for all other shear displacements were nearly identical, indicating that the effective pressure relation is not strongly dependent on displacement. For pure montmorillonite (Figure 7a), the data points cluster together along a single line, regardless of the confining or pore pressures applied. Variations in α above and below a value of 1 cause an immediate divergence of the data points, showing that $\alpha = 1.00 \pm 0.01$ is the best fit. This plot verifies that the effective pressure law for the friction of montmorillonite holds under the pressure conditions tested; the effective pressure in eq. (1) can be written as $P_c - P_p$, and the effective normal stress as $\sigma_n - P_p$. Data for the mixed clay (Figure 7b) and pure illite samples (Figure 7c) also fall along a single trend line for all pressure conditions, indicating that the simple effective pressure law for friction, $P_c - P_p$, holds for these samples as well. This important conclusion verifies that the expandable nature of the montmorillonite does not influence the effective pressure law in a way that differs from the nonexpandable illite.

4.5. Friction

Additional aspects of the strength behavior of these gouges can be gleaned from other details of Figure 7. For instance, the shear and normal stress relation for montmorillonite does not follow a straight line. These data bend upward at effective pressures of around 50-100 MPa, so that the gouge becomes proportionally stronger at the higher pressures. This behavior was observed regardless of shear displacement. The mixed clay (Figure 7b) shows this trend to a lesser degree. Illite, on the other hand, shows no

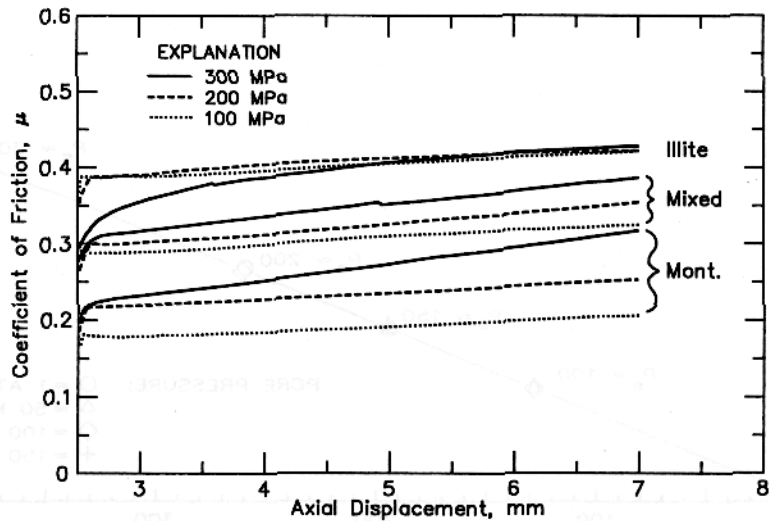


Figure 8. Coefficient of friction as a function of axial displacement for montmorillonite, mixed clay, and illite after sample saturation. Effective pressures indicated in MPa.

variation in the slope of the shear and normal stress relation with effective pressure (Figure 7c). These data follow a straight line that intersects the origin.

The pressure dependence of the shear stress shown in Figure 7 is more clearly demonstrated if we plot the coefficient of friction, $\tau/(\sigma_n)_e$ at selected effective pressures, as shown in Figure 8. The dry portions of the curves are not of interest and have been eliminated, so that displacement begins at 2.5 mm. The coefficient of friction of the montmorillonite is strongly dependent upon effective pressure as noted above, with a range in the friction values from around 0.2 to 0.3 by the end of the experiment for pressures between 100 and 300 MPa. The spread in the friction values diminishes with the addition of illite, as seen in the mixed clay samples. Finally, the coefficients of friction of the pure illite runs are nearly coincident at around 0.4 indicating little dependence on effective pressure, corresponding to the linear relation in Figure 7c. This systematic progression towards a constant coefficient of friction illustrates that as the illite content increases the samples become stronger and the pressure dependence of friction is reduced.

5. Discussion

Frictional sliding experiments conducted on the clay gouges, montmorillonite, and illite verify that the strength of these materials follows the simple effective pressure law. The measured shear stresses depended solely on the difference between the confining and pore pressures $P_c - P_p$, at all pressures and displacements tested. Frictional sliding studies that appear to deviate from this law for montmorillonite and illite are most likely the result of experimental conditions in which the true fluid pressure acting on the material is different from the externally measured pressure. This can easily be caused by the low permeability of these mineral aggregates, which may prevent changes in fluid pressure from equilibrating rapidly. Such a condition was observed by Wang et al. (1979), who reported an apparent pressure independence of strength in montmorillonite

above 200 MPa, which was attributed to high fluid pressures trapped in the clay. It is important to remember that such samples still follow the effective pressure law, even though the true effective pressure acting in the sample is unknown.

One of the questions which we wished to address was whether the expandable nature of the montmorillonite would result in a different frictional behavior from that of the nonexpandable illite. Although the effective pressure law was not sensitive to this difference, the response of the two clays was different, as shown by the nonlinear increase in strength of the montmorillonite at higher effective pressures. This result can be understood if we consider the properties of the bonded water in the montmorillonite.

The hydration phases of montmorillonite have been extensively treated in the literature. Expandable clays can take on numerous layers of bonded water, which cause discrete increases in the d-spacing of the silicate layers (swelling). The interaction of this structural water with the silicate layers creates interlayer forces whose exact origin is a matter of debate (Viani et al., 1983). Bird (1984) measured the pressure stability fields of different hydrated phases, and the shear stresses required to cause slip on each phase at different normal stresses. He found that the shear strength of montmorillonite was greatest in the dehydrated state, and decreased with the addition of each water layer. Since the interlayer forces decay with distance, the first few layers had the most effect on strength. These water layers act as glide planes along which slip can more easily take place, accounting for the fact that expandable clays are weaker than nonexpandable ones. In addition, the water layers can be expelled with applied pressure. The strength of the hydrated phases is also a function of mineral composition. For instance, the hydrated phases of Na-montmorillonite are weaker than those of Ca-montmorillonite, because of the higher concentration of Ca cations in the Ca-montmorillonite. These additional cations form a stronger bond between the silicate layers, which in turn act on the hydrated phase. Since our samples were composed predominantly of Na-montmorillonite, the corresponding strengths for this composition are most relevant to our discussion. Bird (1984) found that for frictional sliding experiment on Na-rich samples, the phase change between the dehydrated and first water layer state occurred in a transitional pressure range of a few tens of MPa centered at an effective normal stress of around 100 MPa. This pressure was higher (~ 180 MPa) and more sharply defined for Ca-rich samples. Above that pressure, a state of dehydration exists in the mineral. The expelled water becomes free water that contributes to the pore pressure. These results are corroborated by the work of Israelachvili et al. (1988), who showed that the physical properties of molecularly thin liquid films are different than those of bulk liquid, and that the frictional force between thinly separated surfaces is a discrete function of the number of boundary layers.

The behavior of bonded water layers under pressure may explain the observed increases in the coefficient of friction of our montmorillonite samples with effective pressure. Shear and normal stress data exhibit a broad inflection point at around 50-150 MPa for the pure montmorillonite (Figure 7a). This inflection point is more clearly defined for the mixed clay (Figure 7b) at around 150 MPa, possibly because of the limited data at the lower pressures compared to the montmorillonite. The change in slope may represent the normal stresses at which the interlayer water is squeezed out under pressure. Above that pressure, the mineral structure does not change further, so that the slope of the shear versus normal stress curve remains constant. Although we do not know the hydration state that existed during our experiments, the behavior of the samples was consistent with Bird's findings. The mixed gouges were less influenced by the expulsion of the

interlayer water, as we might expect, because only half of the sample by weight was composed of an expandable clay. The coefficient of friction of the nonexpandable illite (Figure 7c) was independent of effective pressure.

These results have important implications for the state of stress at depth in fault zones, because they imply that at depths greater than a few kilometers, where lithostatic pressures are squeezing the water out of the clay structure, the relevant coefficient of friction of a montmorillonite gouge will be that of the dehydrated state rather than the expanded state. The true coefficient of friction at depth may be higher than values typically reported in the literature on the basis of measurements made at lower effective pressures. For instance, our measurements below 100 MPa effective pressure gave a coefficient of friction of around 0.2, whereas at 300 MPa the coefficient of friction increased to around 0.3. Although the strengthening of the gouge with pressure does not increase the coefficient of friction to levels near those of crystalline rocks, or even to that of illite ($\mu = 0.4$), this behavior needs to be taken into account if expandable clays are called upon to explain the low strength of faults inferred from heat flow measurements.

Several other details of frictional behavior must be considered when comparing these laboratory results to the in-situ environment. For instance, the velocity step tests show that the gouges may be several percent weaker if shearing takes place at rates comparable to the average San Andreas slip rate. Although this factor contributes to the 'weak gouge' explanation for the low strength of the San Andreas fault, the velocity effects alone are probably insufficient to lower the strengths to the necessary levels (Figure 5). Strain hardening has the opposite effect on strength, particularly at the higher effective pressures. Strength increased substantially with displacement for all of the gouge types studied. Since this scales with strain rather than total slip, the strain hardening may not be as significant for slip on thick natural faults as compared to laboratory experiments. The strain hardening behavior renders a definitive measurement of gouge strength difficult, because it is not clear from these triaxial tests at what point the samples will reach a steady-state stress level. Clearly, the strain hardening can not go on forever. At best, we can compare the relative strengths of the gouges at a given strain. Finally, these room-temperature experiments do not take into account the effects of increasing temperature with depth in the earth. Moore et al. (1989) found that the strength of heated illite gouges increased with temperature owing to greater degrees of induration of the particles. This might suggest that our laboratory measurements are an underestimate of the true in-situ strength. Other temperature effects that might be relevant in the in-situ environment include a change in deformation mechanism, change in velocity dependence, reactions to stronger or weaker products, and ductility.

Although the limitations of the laboratory data are apparent from the discussion above, these experimental results are nonetheless sufficiently relevant to address the final and most important question we wish to consider. That is, how do the measured shear stresses of the clay gouges compare with the average shear stresses to seismogenic depth? Two cases are considered, both with the condition that fluid pressures remain hydrostatic with depth. The first case assumes that montmorillonite undergoes a phase transformation to illite with increasing pressure. This view is generally supported by geologic evidence in other natural environments. For this model, the stress levels given in Figures 7a-c for montmorillonite at low pressure, mixed clay at mid-pressure, and illite at high pressure are plotted over a depth interval of 0-15 km (Figure 9, mixed symbols). Clearly the exact shape of this profile will depend on the depth range of the

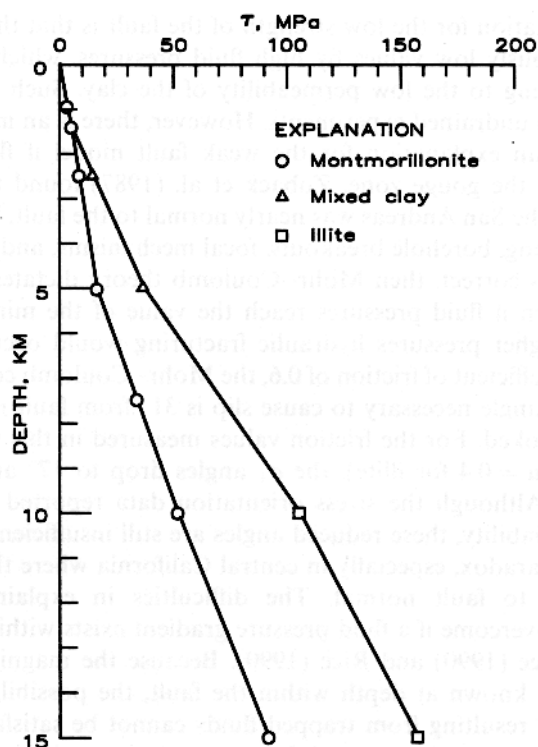


Figure 9. Selected shear stress data from Figure 7 as a function of depth for the case of montmorillonite undergoing a phase change to illite (mixed symbols), and the case of montmorillonite remaining stable with depth (round symbols). Temperature effects with depth are not considered in this plot.

mineral transition and the proportion of the endmember clays at intermediate depths. However, integrating the stress values from these experiments with depth yields an average shear stress of around 60 MPa in the crust. This value is higher than the 10-20 MPa prescribed by heat flow measurements, seismic stress drops and in-situ testing, so that this clay profile alone is insufficient to explain the existence of a weak fault.

The other case pertinent to the discussion of fault strength assumes that montmorillonite, the weaker of the two minerals, persists at depth. For the case of stable montmorillonite, Figure 7a is relevant over all pressures studied (Figure 9, round symbols). Integrating these measurements over the depth to the seismogenic zone gives an average shear stress value of around 30 MPa. This is still higher than the assumed in-situ stress state of 10-20 MPa. This result would not be anticipated if the laboratory stress measurements made at low effective pressures were extrapolated to higher pressures, because of the nonlinear relation between strength and pressure. The implication of these calculations is that the presence of low-strength clay minerals cannot be reconciled with the stress-heat flow paradox if the gouges are under normal hydrostatic pressures, no matter what the composition with depth, because the clay gouges are stronger than the prescribed state of stress on the fault. If strain hardening or temperature effects are considered, the average shear strength of the clay could be even higher still.

One possible explanation for the low strength of the fault is that the strength of clay is reduced to anomalously low values by high fluid pressures, which become trapped in the gouge zone owing to the low permeability of the clay. Such low strengths are commonly observed in undrained experiments. However, there is an important problem with this concept as an explanation for the weak fault model if fluid pressures are uniformly high within the gouge zone. Zoback et al. (1987) found that the principal stress direction along the San Andreas was nearly normal to the fault, based on evidence from hydraulic fracturing, borehole breakouts, focal mechanisms, and geologic features. If this interpretation is correct, then Mohr-Coulomb theory dictates that slip cannot occur on the fault even if fluid pressures reach the value of the minimum horizontal principal stress (at higher pressures hydraulic fracturing would occur in the country rock). For a typical coefficient of friction of 0.6, the Mohr-Coulomb construction shows that the minimum σ_1 angle necessary to cause slip is 31° from fault normal when high fluid pressures are invoked. For the friction values measured in this study ($\mu \sim 0.3$ for montmorillonite and $\mu = 0.4$ for illite), the σ_1 angles drop to 17° and 22° from fault normal, respectively. Although the stress orientation data reported by Zoback et al. (1987) show some variability, these reduced angles are still insufficiently low to explain the stress-heat flow paradox, especially in central California where the principal stress directions are closer to fault normal. The difficulties in explaining fault-normal compression may be overcome if a fluid pressure gradient exists within the gouge zone, as proposed by Byerlee (1990) and Rice (1990). Because the magnitudes of the fluid pressures are not well known at depth within the fault, the possibility of abnormally low effective pressures resulting from trapped fluids cannot be satisfactorily addressed at present. Clearly, the factors that control the stresses and constitutive properties along the San Andreas fault must be further explored in order to resolve the long standing stress-heat flow debate.

6. Conclusions

- (1) The effective pressure law for friction holds under all pressure conditions for both the montmorillonite and illite gouges. The measured shear stresses were a function of the effective pressure, $P_c - P_p$, independent of the particular choice of confining and pore pressures.
- (2) Pure montmorillonite gouge was the weakest of the gouge types studied. Shear strength increased with increasing illite content. Dry gouges were consistently stronger than the saturated gouges.
- (3) The coefficient of friction of the montmorillonite gouge was dependent on effective pressure, increasing at higher pressures, whereas the illite gouge showed no dependence on effective pressure. We suggest that this behavior is caused by the presence of loosely bonded interlayer water in the montmorillonite that is squeezed out at the higher pressures, causing an increase in strength. The nonexpanding illite gouge is not influenced in this way.
- (4) The average shear stresses of both the illite and montmorillonite gouges measured over pressures simulating depths to the seismogenic zone were greater than the average stresses along the San Andreas fault inferred from heat flow measurements and borehole stress measurements. Therefore, the low strength of these clay gouges under normal hydrostatic conditions is insufficient to account for the weak fault model.

References

- Bird, P. (1984). Hydration-phase diagrams and friction of montmorillonite under laboratory and geologic conditions, with implications for shale compaction, slope stability, and strength of fault gouge. *Tectonophysics* **107**, 235-260.
- Brace, W.F. (1972). Pore pressure in geophysics. In *Flow and Fracture of Rocks* (eds. H.C. Heard, I.Y. Borg, N.L. Carter, and C.B. Raleigh), pp. 265-273. American Geophysical Union Geophysical Monograph No. 16.
- Brace, W.F. and Martin, R.J. (1968). A test of the effective stress law for crystalline rocks of low porosity. *Int. J. Rock Mech. Min. Sci.* **5**, 415-426.
- Byerlee, J.D. (1967). Frictional characteristics of granite under high confining pressure. *J. Geophys. Res.* **72**(14), 3639-3648.
- Byerlee, J. (1978). Friction of rocks. *Pure Appl. Geophys.* **116**, 615-626.
- Byerlee, J. (1990). Friction, overpressure and fault normal compression. *Geophys. Res. Lett.* **17**(12), 2109-2112.
- Colten-Bradley, V.A. (1987). Role of pressure in smectite dehydration-effects on geopressure and smectite- to -illite transformation. *Am. Assoc. Pet. Geol. Bull.* **71**(11), 1414-1427.
- Freed, R.L. and Peacor, D.R. (1989). Variability in temperature of the smectite/illite reaction in gulf coast sediments. *Clay Minerals* **24**, 171-180.
- Garg, S.K. and Nur, A. (1973). Effective stress law for fluid saturated rocks. *J. Geophys. Res.* **78**(26), 5911-5921.
- Israelachvili, J.N., McGuiggan, P.M., and Homola, A.M. (1988). Dynamic properties of molecularly thin liquid films. *Science* **240**, 189-190.
- Lachenbruch, A.H. and Sass, J.H. (1980). Heat flow and energetics of the San Andreas fault. *J. Geophys. Res.* **85**, 6185-6222.
- Logan, J.M. and Rauenzahn, K.A. (1987). Frictional dependence of gouge mixtures of quartz and montmorillonite on velocity, composition and fabric. *Tectonophysics* **144**, 87-108.
- Meunier, A. and Velde, B. (1989). Solid solutions in I/S mixed-layer minerals and illite. *Am. Mineral.* **74**, 1106-1112.
- Moore, D.E., Ma Jin, Summers, R., and Byerlee, J. (1984a). The effects of strain rate and pore pressure on the strength of heated fault gouge. *EOS* **65**, 1078.
- Moore, D.E., Ma Jin, Summers, R., and Byerlee, J. (1984b). The effect of pore pressure and heating time on the strength and stability of a serpentine gouge. In *Rock Mechanics in Productivity and Protection*, Proc. 25th Symp. on Rock Mech. (eds. F. Dowding and M. Singh), pp. 312-319.
- Moore, D.E., Summers, R., and Byerlee, J. (1989). Sliding behavior and deformation textures of heated illite gouge. *J. Struct. Geol.* **11**(3), 329-342.
- Morrow, C.A. and Byerlee, J.D. (1989). Experimental studies of compaction and dilatancy during frictional sliding on faults containing gouge. *J. Struct. Geol.* **11**(7), 815-825.
- Morrow, C.A., Shi, L.Q., and Byerlee, J.D. (1982). Strain hardening and strength of clay-rich fault gouge. *J. Geophys. Res.* **87**(B8), 6771-6780.
- Morrow, C.A., Shi, L.Q., and Byerlee, J.D. (1984). Permeability of fault gouge under confining pressure and shear stress. *J. Geophys. Res.* **89**(B5), 3193-3200.
- Nur, A. and Byerlee, J.D. (1971). An exact effective stress law for elastic deformation of rocks with fluids. *J. Geophys. Res.* **76**(26), 6414-6419.
- Rice, J.R. (1990). Fault stress states, pore pressure distributions, and the weakness of the San Andreas fault. *EOS* **71**(43), 1652.
- Robin, P.F. (1973). Note on effective pressure. *J. Geophys. Res.* **78**(14), 2434-2437.
- Summers, R. and Byerlee, J. (1977). Summary of results of frictional sliding studies, at confining pressures up to 6.98 kb, in selected rock materials. U.S. *Geological Survey, Open File Report 77-142*.
- Viani, B., Low, P., and Roth, C. (1983). Direct measurement of the relation between interlayer force and interlayer distance in the swelling of montmorillonite. *J. Colloid Interface Sci.* **96**(1), 229-244.

- Wang, C.Y. and Mao, N. (1979). Shearing of saturated clays in rock joints at high confining pressures. *Geophys. Res. Lett.* **6**(11), 825-828.
- Wang, C.Y., Mao, N., and Wu, F.T. (1979). The mechanical property of montmorillonite clay at high pressure and implications on fault behavior. *Geophys. Res. Lett.* **6**(6), 476-478.
- Wang, C.Y., Mao, N., and Wu, F.T. (1980). Mechanical properties of clays at high pressure. *J. Geophys. Res.* **85**(B3), 1462-1468.
- Wang, C.Y. (1984). On the constitution of the San Andreas fault zone in central California. *J. Geophys. Res.* **89**(B7), 5858-5866.
- Wu, F.T., Blatter, L. and Robertson, H. (1975). Clay gouges in the San Andreas fault system and their possible implications. *Pure Appl. Geophys.* **113**, 87-95.
- Wu, F.T. (1978). Mineralogy and physical nature of clay gouge. *Pure Appl. Geophys.* **116**, 655-689.
- Zoback, M.D. and Byerlee, J.D. (1975). Permeability and effective stress. *Bull. Am. Assoc. Pet. Geo.* **59**(1), 154-158.
- Zoback, M.D., Zoback, M.L., Mont, V.S., Suppe, J., Eaton, J.P., Healy, J.H., Oppenheimer, D., Reasenber, P., Jones, L., Raleigh, C.B., Wong, I.G., Scotti, O., and Wentworth, C. (1987). New evidence on the state of stress of the San Andreas fault system. *Science* **238**, 1105-1111.